The Monte Carlo Method: Versatility Unbounded in a Dynamic Computing World
Chattanooga, Tennessee, April 17-21, 2005, on CD-ROM, American Nuclear Society, LaGrange Park, IL (2005)

BENCHMARK STUDY OF RADIONUCLIDE PRODUCTION WITH FLUKA

M. Brugger, S. Roesler and L. Ulrici
CERN, SC-RP
CH-1211 Geneva 23
Switzerland
Markus.Brugger@cern.ch

ABSTRACT

Samples of different materials to be used for machine and shielding components of the Large Hadron Collider were irradiated in a high-energy stray radiation field. The induced specific activities of radionuclides, as measured with gamma spectrometry, then served as benchmark of the FLUKA Monte Carlo code. The study aimed at high accuracy in all aspects of measurements and simulations, including elemental analyses of the irradiated materials with different methods, detailed revision of the spectrometry results as well as low statistical uncertainties in the predictions of FLUKA. Furthermore, the production and decay channels leading to the various radionuclides were determined in the simulations allowing a detailed investigation of the benchmark results. The study demonstrates that the models implemented in FLUKA are able to predict the production of individual radionuclides to within 30% accuracy in many cases. It underlines the necessity to keep the uncertainties of both experimental and calculational aspects of benchmark studies below that level to allow meaningful conclusions. Finally, a new implementation of the evaporation of fragments is evaluated and shows promising results.

Key Words: Induced radioactivity, high energy accelerators, Monte Carlo simulation

1 INTRODUCTION

The operation and decommissioning of high energy accelerators requires detailed estimations of induced radioactivity in order to keep the impact on personnel and environment as low as reasonably achievable. Modern particle interaction and transport codes, such as FLUKA [1, 2], allow detailed calculations of the radionuclide inventory and thus the optimization of the accelerator design in this respect. The accuracy of the predictions is usually determined with benchmark measurements.

Recently a series of experiments was performed at the CERN-EU high energy Reference Field (CERF) facility [3] in which samples of materials used for machine and shielding components of the Large Hadron Collider (LHC) were irradiated in a high energy stray radiation field. First results on measured specific activities were reported in Refs. [4, 5] and compared to predictions obtained with the FLUKA code. It was shown that for many radionuclides the measured and calculated values agreed to within 30%. In a few cases, however, discrepancies were observed and associated to either deficiencies in the models or to uncertainties in the measurements and data analysis.

The results underlined again the complexity of such benchmark studies where meaningful conclusions can only be obtained if measurement uncertainties as well as uncertainties arising from approximations in the simulation of the irradiation experiment are well within the accuracy of the models to be tested. Furthermore, it is often difficult to generalise conclusions for several reasons: Results are specific to the particle composition and energy spectrum of the irradiation field of the experiment. The production of certain isotopes could be dominated by spallation reactions in a field dominated by high energy particles or result mainly from low energy neutron interactions if the radiation field is dominated by neutrons. In addition, radionuclides measured at a certain decay time might be product of radioactive decays rather than being directly produced by high energy interactions.

Detailed information on the reaction channels and energy ranges tested with a certain activation measurement can, however, be obtained from the simulation. This is demonstrated in the present study for three selected materials (concrete, copper and aluminum) of the above mentioned irradiation experiments. By reducing and/or avoiding uncertainties and by analysing production channels, specific conclusions on the quality of the FLUKA predictions for certain isotope production cross sections are possible. In the following, emphasis is put on the methods rather than giving a global overview over the results for all irradiated samples.

2 BENCHMARK MEASUREMENTS

A total of 22 samples of 14 different materials were irradiated in the stray radiation field created by a 120 GeV beam of positively charged hadrons in the copper target (50 cm long and 7 cm in diameter) of the CERF facility. The samples were either placed downstream of the target, centered with its axis, or were attached laterally, approximately in the maximum of the hadronic shower. After the irradiation the radioactivity induced in the samples was analysed at different cooling times with gamma spectrometry measurements. In the following, details are given only for the three samples subject to this study. Further information about the samples and the setup of the experiment can be found in Ref. [5].

2.1 Irradiation Experiment

The copper and aluminum samples were selected from the LHC material catalogue and machined to a cylindrical size of 2 cm length and diameter. The concrete sample, originating from the LHC tunnel wall at octant 7, was powdered and filled into cylindrical boxes of 4 cm length and diameter. The copper and concrete samples were placed at downstream irradiation locations whereas the aluminum sample was attached laterally to the target, about 30 cm downstream of its front face. The irradiation period included six days of varying beam intensity recorded with a beam monitor for each pulse from the Super Proton Synchrotron (SPS)-accelerator (cycle period of 16.8 s). The irradiation profile, shown in Fig. 1, was taken into account in the calculation of the build-up of the activation (see below). As can be seen, periods of constant intensity were concentrated towards the end with only 30% of the total number of beam particles accumulated during the first half of the irradiation period. This underlines the importance of calculating the isotope build-up based on the actual profile, especially for isotopes with half-lives up to one week. The uncertainty of the monitor reading is about 10% (see Ref. [3] and references therein).

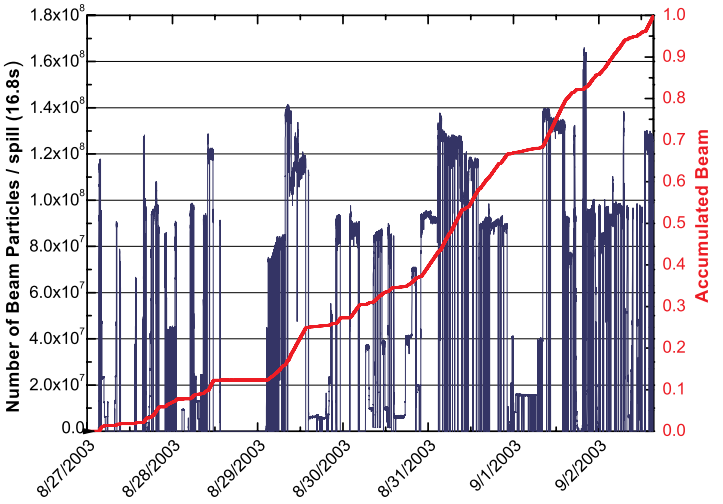

Figure 1: Profile of the irradiation of the samples. The number of beam particles in each spill (left scale) is shown together with the accumulated fraction of the total number of beam particles (right scale).

The FLUKA simulations required detailed information on the elemental composition. Thus, material samples were sent to an external institute* and external companies† for analysis. The resulting compositions are given as fractions of weight in Table I. In order estimate the systematical uncertainties of the used methods, in case of aluminum different laboratories were asked to perform an analysis: EMPA and EIG using X-ray Fluoresence (XRF) spectrometry, and EA with Optical Emission spectrometry. As shown in Table I the weight fractions of trace elements can differ significantly. Therefore, it was decided to base the simulations on average weight fractions and to include all trace elements detected with the two methods unless only upper limits were given. In case of concrete, different analysis methods were applied: the weight fractions of oxygen and carbon were determined by weight measurements during a staged heating process, other elements were measured with wavelength-dispersive XRF spectrometry. Furthermore, although europium was detected it was not included in the present study it was found that the build-up during the given irradiation period was too small.

2.2 Gamma Spectrometry Analysis

The specific activities of the irradiated samples were measured at different cooling times ranging from 20 minutes to two months. The gamma spectrometry measurements were performed with a high sensitivity, low background HPGe detector by Canberra‡ (245 cm^3 sensitive volume, efficiency of 60% at 1.33 MeV). The data acquisition and analysis was carried out using the software GENIE 2000 (version 2.1) by Canberra and the PROCOUNT-2000 counting procedure

*Ecole d'Ingénieurs - hes Genève EIG, 4, rue de la Prairie, CH-1202 Genève, Switzerland

†Elemental Analysis Corporation, 101 Venture Ct., Lexington, KY 40511, U.S.A., EMPA, Überlandstrasse 129, CH-8600 Dübendorf, Switzerland

‡CANBERRA/EURISYS S.A., 4 Avenue des Frenes, 78067 St. Quentin Yvelines, France

software.

During the measurement the samples were positioned on an appositely built sample holder at different reproducible distances, chosen for each sample on the basis of its remanent dose rate, thus on the average dead time expected during the gamma spectroscopy. The efficiency of the detector at the respective distances, also including the sample dimensions and material properties, was calculated using LABSOCS (Laboratory SOurceless Calibration Software, by Canberra, version 4.1.1), a mathematical efficiency calibration software taking into account geometrical effects and self-absorption in the samples

The automatic analysis performed by the software package includes advanced analysis algorithms for the nuclide identification (by standard or user-generated libraries): interference correction (resolution of overlapping peaks into individual components), calculation of the specific activities and background subtraction as well as efficiency correction.

In order to achieve the most accurate result, for this study user-specific libraries were generated for each sample material taking into account the chemical composition, the possible activation reactions and the time elapsed between the end of the irradiation and the gamma spectrometry measurement. In case isotopes not included in this library but present in the sample, the analysis procedure would list the corresponding gamma lines as so-called “unidentified peaks”, thoroughly checked for each analysis.

In order to consider also the decay of isotopes during or in-between consecutive measurements, leading to daughter isotopes also being radioactive gamma-ray emitter, the software package includes a correction usually known as “Parent-Daughter Correction”. This is of particular importance for isotopes for which the build-up from metastable states plays a significant role, *i.e.* where the half-life of the mother isotope corresponds to the respective cooling time. Unfortunately, this module in GENIE 2000 still contains unresolved problems, thus leads to significant errors when applied to cases where the reference time for the analysis becomes comparable to the time of the counting (*e.g.*, the start of the measurement). So far, this error could not be consistently fixed, thus it was decided not to apply this method for this study, but only to discuss the respective isotope case-by-case and perform manual calculations.

Furthermore, in case of other ambiguities the results of the automatic analyses made by GENIE 2000 were systematically manually revised. For some radionuclides (*e.g.*, in case of interference in the gamma emissions) the manual calculation of the specific activity turned out to be the most accurate approach. For example, ^{60}Cu is usually detected mainly using three different gamma lines (826.5, 1333.0, 1791.6 keV, respectively), however showing a difficult combination of other possible contributing isotopes (^{60}Co and ^{52}Mn), which cannot always be correctly resolved by the analysis code. Therefore, a manual correction to the library selecting the isolated line coming only from ^{60}Cu (1791.6 keV), even having a comparably low yield, enables distinguishing between the different contributors, thus results in the correct measured activity.

The Minimal Detectable Activity (MDA) is computed for each isotope by an evaluation algorithm included in GENIE 2000 following the Currie method [6]. It corresponds to a 95% confidence level above the detection limit and gives a measure of the confidence in the measured activity. Values below the MDA value thus include high uncertainties and were excluded further in this study.

3 DETAILS OF THE CALCULATIONS

The present study benchmarks FLUKA2002 in its version 4.0 (release April 2003), below referred to as "FLUKA def" and FLUKA2003 version 1.0b (release March 2004) with a new evaporation treatment, in the following referred to as "FLUKA new".

3.1 Radionuclide Production with FLUKA

Different models are implemented in FLUKA for the description of nuclear reactions, see Ref. [7] for a recent review. High energy collisions ($E > 5$ GeV) are treated within a Glauber-Gribov formalism coupled to a generalized intranuclear cascade model. Interactions at lower energies are simulated according to a very detailed intranuclear cascade model smoothly joined to a statistical preequilibrium emission. In both cases excited prefragments may evaporate light nuclei ($A \leq 4$) and emit photons during deexcitation into their ground state. For light nuclei ($A < 18$), a Fermi break-up model is implemented. Recently, the evaporation of nuclear fragments has been extended to include mass numbers up to $A = 24$ [7]. Therefore, considerable improvements for predictions of radionuclides in the multifragmentation region can be expected and first results were reported in Ref. [7].

The implemented models allow an explicit simulation of the production of individual radionuclides (and, therefore, also of the corresponding cross sections) for hadrons of all energies except low energy neutrons ($E < 20$ MeV). Reactions of the latter are not treated explicitly but experimental cross sections for scattering and radionuclide production are used instead.

All radionuclide production cross sections discussed in the following were calculated with a non-standard FLUKA routine [8]. It calls directly the inelastic interaction models for a given combination of projectile, target nucleus and energy and allows scoring of individual residual nuclei. It returns the inelastic cross section as well as individual radionuclide production cross sections.

3.2 Simulation of the Irradiation Experiment

The simulations are based on a detailed geometrical implementation of the CERF facility, including sample holders and concrete enclosure of the beamline shielding. All samples were defined with their actual size and elemental composition (see Table I). Beam profile measurements returned the full width at half maximum (FWHM) of the approximately Gaussian beam shape. The latter together with the measured small offset between the axes of the beam and the CERF target were appropriately taken into account in the calculations.

Separate simulations were performed for the proton and positively charged pion component of the CERF beam and results were combined offline (65.2% π^+, 34.8% p). Possible deviations from the actual beam composition, including the neglect of the kaon component, were found to have negligible influence on the results. In order to keep statistical uncertainties on the production of individual radionuclides within a few percent, results were averaged over hadronic cascades caused by about 7-10 Million beam particles of each type.

Each calculation included the scoring of both radionuclide yields and energy spectra of protons, neutrons and charged pions, to allow off-line folding of spectra with energy-dependent

radionuclide production cross sections. The spectra revealed strong dependence on sample material and location. Figure 2 shows the fluence spectra in the aluminum and copper samples. Note, that the former was attached laterally to the target, whereas the latter was irradiated downstream of it, explaining the differences between them, in particular in the high energy range.

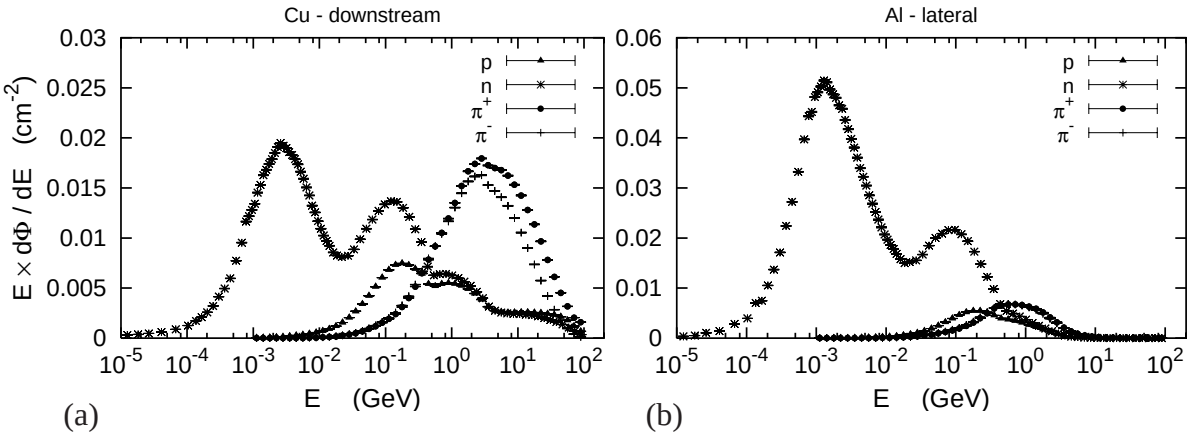

Figure 2: Fluence spectra of protons, neutrons and charged pions at the location of the copper (a) and aluminum samples (b).

3.3 Data Analysis

In order to identify which reaction channels contribute to the production of a certain isotope additional scoring was implemented and data analysis performed. Two mechanisms can be distinguished, direct production of the radionuclide in interactions of the particle shower in the samples and indirect production through decays of radioactive parent-nuclei. The former contribution was determined by scoring of the reaction (projectile hadron and target nucleus) every time a residual nucleus is produced in the shower. On the other hand, post-processing of the FLUKA output from the residual nuclei scoring allowed the identification of the radioactive decay chains. This step in the off-line data analysis included the calculation of the nuclide build-up during the irradiation taking into account the actual profile (see Figure 1) as well as of the radioactive decay, both including decay chains up to several generations [9].

Different isomeric states of a certain radionuclide cannot be separately predicted by FLUKA. In this case the post-processing algorithm assumes equal sharing of the nuclide yield between the different states and calculates build-up and decay correspondingly. The sensitivity of this assumption on the final results will be discussed below.

Furthermore, energy-dependent cross sections were calculated with FLUKA for the most important reactions as identified with the above mentioned scoring. Folding of these cross sections with the fluence spectra for the sample locations then allowed to determine the energy range tested with the activation measurement (“response”). In addition, nuclide yields produced with very low probability in the shower simulation (thus showing large statistical uncertainties) can be obtained with this method with low uncertainty provided that the parent nucleus is known.

4 COMPARISON OF MEASURED AND CALCULATED SPECIFIC ACTIVITIES

In the following, calculated and measured specific activities are compared for a cooling time corresponding to the start of the respective gamma spectrometry measurement. This choice allowed to reduce as much as possible the effect of ambiguities in the treatment of radioactive decay chains by the gamma spectrometry software (see Section 2.2). Nevertheless the problem of the gamma spectrometry analysis should be kept in mind when drawing conclusions for certain nuclides, *e.g.*, in case of isomer decay.

Typically 3-4 gamma spectrometry measurements were performed for each sample covering cooling times between several minutes to several months. Many isotopes were detected at different cooling times and their specific activities were determined. However, for the final comparison with FLUKA predictions only one measurement result was selected for each nuclide based on the following criteria: smallest experimental uncertainty, lowest ratio between measured activity and MDA and comparability of cooling time and half-life. The experimental errors contain both statistical and systematic uncertainties whereas for calculated values only statistical uncertainties are given. Calculated activities with uncertainties exceeding 10% are considered to be unreliable as the estimate (standard deviation over batches of simulations) might underestimate the actual error. Values with errors above 20% were excluded from the comparison.

The results for the three materials are given in Tables II-IV. The header notation "MDA ratio" refers the ratios of measured activity and MDA; nuclides with ratios below unity were excluded.

4.1 Copper Sample

The FLUKA results for the copper sample (see Table II) carry statistical uncertainties of less than 2% in most cases and should thus be reliable in this respect. The new evaporation model largely improved predictions for low-mass radionuclides (*e.g.*, ^{7}Be, ^{22}Na, ^{24}Na). For higher masses, FLUKA results and measured specific activities agree to within 20% for many isotopes. In only a few cases the activities calculated with the new evaporation model over- or underestimate the measured values by more than 30%. **^{m52}Mn/^{52}Mn:** As mentioned above, FLUKA cannot predict the production of different isomers which might contribute to the observed discrepancies. **^{65}Ni:** This is one of the few isotopes for which the measured activity is rather close to the MDA reflected by a correspondingly large experimental error. **^{64}Cu:** The cross section for the production of this isotope seems to be underestimated. In addition, low-energy neutron interactions and thermal neutron capture reactions contribute about 50% to the total yield. Thus, uncertainties in the simulation of the material in the close vicinity of the sample (supports, concrete shielding, *etc.*) might also be reasons for the discrepancy. **^{65}Zn:** The result could indicate an underestimation of the cross section for the production of this isotope in proton and positively charged pion interactions on ^{65}Cu.

4.2 Concrete Sample

The observed agreement for most of the isotopes (see Table III) supports the observation that a meaningful benchmark of a Monte Carlo code on isotope production requires the reduction of experimental uncertainties (elemental composition of the sample, irradiation pattern and overall

normalization, gamma spectrometry analysis, *etc.*) to below those of the model predictions. Again, the discrepancies exceed 30% only in a few cases. ^{24}**Na:** The downstream location of the sample, characterized by a significant fluence of high energy hadrons, explains that this isotope is mainly produced in spallation reactions. Therefore, many elements in the composition of the sample contribute making sound conclusions difficult. ^{m44}**Sc**/^{44}**Sc:** The discrepancy could be due to uncertainties in predicting isomer production. ^{48}**V:** The FLUKA predictions improved with the new evaporation model. However, since this isotope is produced in spallation reactions on iron traces uncertainties in the elemental composition might contribute to the remaining disagreement. ^{51}**Cr,** ^{52}**Mn:** Also these isotopes are produced in reactions on iron nuclei. The overestimation by the simulations supports the observation that the iron content in the sample might be overestimated.

4.3 Aluminum Sample

All isotopes in Table IV with masses larger than that of sodium are produced on trace elements. Results are thus subject to uncertainties in the elemental composition. Except for ^{57}Co and ^{58}Co, which result from interactions on copper and nickel traces, isotopes are created in reactions on titanium, manganese and iron. As Table I indicates the uncertainty in the determination of the mass fractions of trace elements (variations of 30-50% within the different analyses) are considered to be one the main reasons for observed discrepancies between measured and calculated activities. Furthermore, in many cases the measured activities are close to the MDA and carry a correspondingly large error (^{44}Sc, ^{57}Co, ^{58}Co). Again, the new evaporation model improved the results for light isotopes, here for ^{7}Be.

5 ANALYSIS OF RADIONUCLIDE PRODUCTION WITH FLUKA

As mentioned earlier (see Section 3.3) online scoring of reaction channels, folding of fluence with nuclide production cross sections and the identification of radioactive decay channels provided the basis for a detailed analysis of the results. In particular, it allows to determine the reaction cross sections (including the energy range) benchmarked with each gamma spectrometry measurement. In the following, the overall strategy is explained by giving a few examples. Similar analyses (not shown here) are available for most of the identified radionuclides.

5.1 Production Channels

The calculation of radionuclide production in FLUKA proceeds either on the basis of models simulating explicitly the interaction and, thus, the creation of residual nuclei or fragments (in the following referred to as “high energy reaction”), or – in case of neutrons with energies below 19.6 MeV – by using tabulated experimental data. In cases where the latter are missing for a certain reaction channel nuclide production by low energy neutron interactions cannot be predicted with FLUKA.

Examples for the contributions from various reactions to the specific activity of a certain nuclide are given in Table V, in the upper part for interactions in the aluminum sample and in the lower part for reaction channels in the copper sample. All values are in percent and have to be read as follows (demonstrated on ^{60}Co produced in copper): 9.7% of the *directly* produced ^{60}Co

yield is caused by low-energy neutron interactions, most likely on trace elements in the sample (low-energy neutron reaction channels were not identified explicitly); the majority of the yield (90.3%) results from high energy reactions. The latter are shared to about equal parts between interactions on the two stable isotopes in natural copper, ^{63}Cu and ^{65}Cu. Of these reactions 17.4% are neutron-^{63}Cu interactions, 16.4% π^--^{65}Cu interactions, *etc.* In addition, ^{60}Co is produced to a small fraction *indirectly* in β^--decay chains of ^{60}Mn and ^{60}Fe. The assumption that the ^{60}Co yield produced directly by FLUKA is shared to equal parts between the isomeric states has no influence on the results due to the long cooling time before the gamma spectrometry measurement (approx. 48 days) as compared to the half-life of $^{\mathrm{m}60}$Co ($t_{1/2}$=10.5m).

5.2 Isotope Production Cross Sections

In order to investigate if the conclusions of the comparison of measured and calculated activities are also reflected by the nuclide production cross sections (for which experimental data may exist) the latter were calculated with a non-standard FLUKA routine as explained above. In addition, the energy-dependent cross sections were multiplied with the calculated particle fluence spectra for the location of the respective sample (see Fig. 2) to obtain information on the energy range to which the activation measurement was sensitive. The energy-dependent product of isotope production cross section and fluence, $\sigma(E) \times d\Phi(E)/dE$, will be referred to as "response". A few reaction channels were selected and are discussed in the following.

As shown in Tables II-IV the predictions for light nuclides, in particular for ^{7}Be, have improved significantly with the new implementation of evaporation processes. This is also reflected by the cross section as shown in Fig. 3a) for proton-induced production of ^{7}Be on

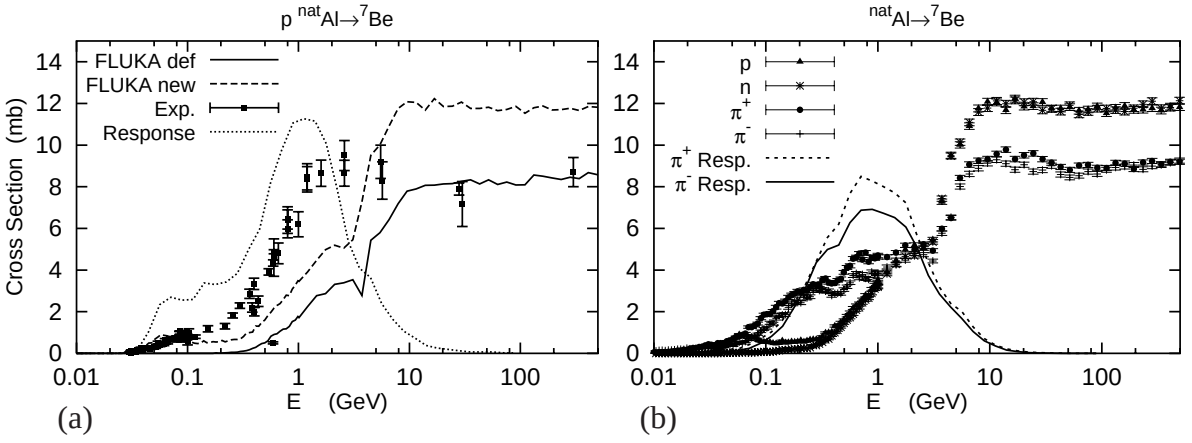

Figure 3: Cross sections for the production of ^{7}Be from natural aluminum. (a) FLUKA-predictions for proton-induced interactions obtained with the default and new evaporation models are compared to experimental data [10]. In addition the response (cross section multiplied with the energy spectrum as shown in Fig. 2b) is given (arbitrary units). (b) The FLUKA cross sections for proton-, neutron- and pion-induced reactions calculated with the new evaporation model is shown together with the response to pions (arbitrary units).

aluminum. The graph compares FLUKA predictions obtained with the default and new

evaporation models to experimental data [10]. As can be seen, despite the increase in the cross section the experimental data are still underestimated, in agreement with the result of the activation benchmark (ratio of calculated over measured activity of 0.72, see Table IV). The response curve (dotted line in Fig. 3a, arbitrary normalization) indicates that the present benchmark experiment is sensitive to an energy range peaked at about 1 GeV. Furthermore, Fig. 3b shows the cross sections predicted by FLUKA with the new evaporation model for various hadrons interacting with aluminum. Here, the response curves are given for charged pions indicating again the energy range between several 100 MeV to several GeV (average energy of protons and pions in the stray radiation field laterally to the CERF target) which was benchmarked in this study.

On the other hand, the cross section for the production of ^{22}Na from aluminum should not have changed with the new evaporation model. This observation is confirmed by the cross sections shown in Fig. 4. Experimental cross section data for proton-induced reactions are underestimated by FLUKA by about 30% (Fig. 4a), in agreement with the ratio of calculated and

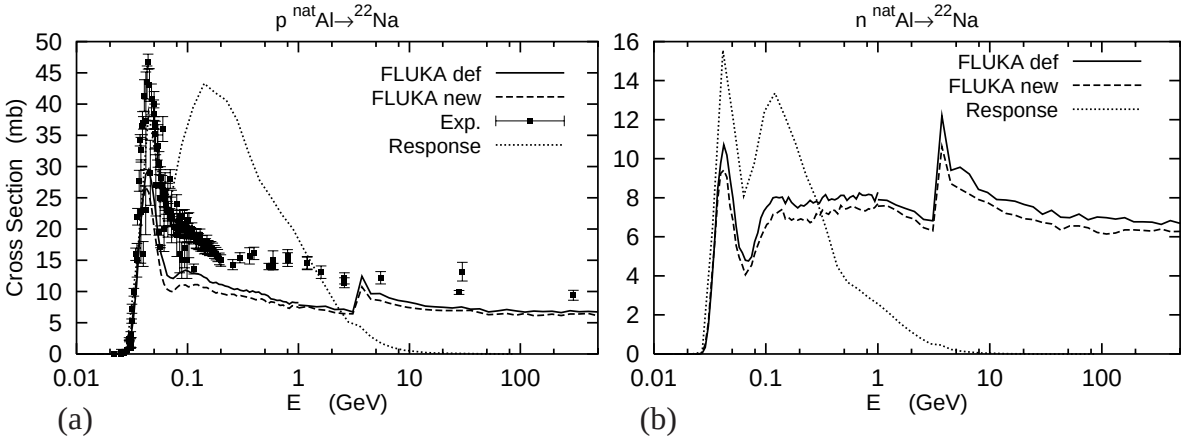

Figure 4: Cross sections for the production of ^{22}Na from natural aluminum. (a) FLUKA-predictions for proton-induced interactions obtained with the default and new evaporation models are compared to experimental data [10]. In addition the response (cross section multiplied with the energy spectrum as shown in Fig. 2b) is given (arbitrary units). (b) The FLUKA cross section for neutron-induced reactions calculated with the default and new evaporation models is shown together with the response curve (arbitrary units).

measured specific activities (ratio of 0.76, see Table IV). The latter indicates that also the cross sections for pion- and neutron-induced reactions must be underestimated by FLUKA since more than 80% of all reactions leading to ^{22}Na are due to the latter particles (see Table V). The discontinuity in the cross section at about 3-5 GeV is caused by the abrupt transition in FLUKA between the low energy and high energy interaction models (see Sec. 3.1). As ^{22}Na is the main contributor to the residual dose rates from induced radioactivity in aluminum at long cooling times the dose rate should be slightly underestimated when calculated with FLUKA.

Although experimental cross sections for pion-induced reactions are not available for many reaction channels, data exist for the production of ^{54}Mn on copper [10]. The latter as well as data

for proton-induced interactions are compared to FLUKA predictions in Fig. 5 and show good agreement which is also confirmed by this study (see Table II). The response curves indicate that

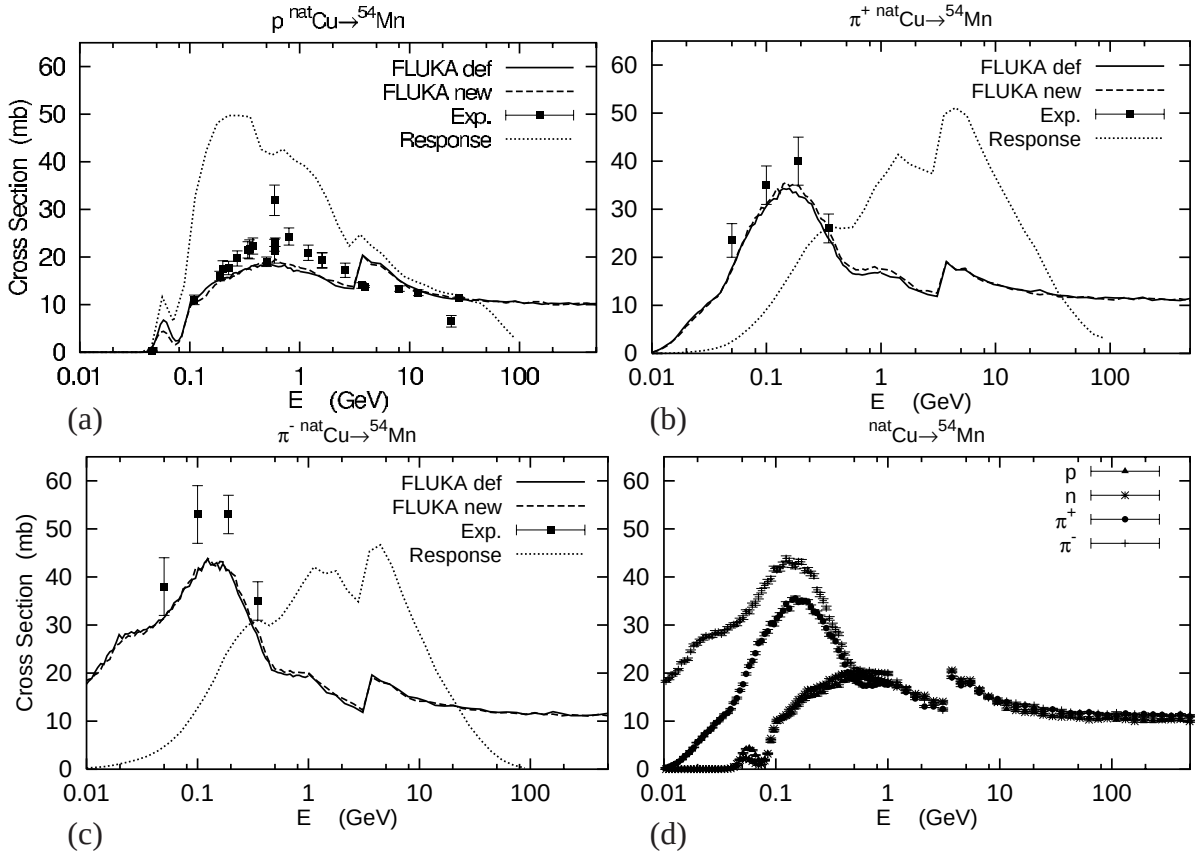

Figure 5: Cross sections for the production of ^{54}Mn from natural copper. FLUKA-predictions for proton- (a), π^+- (b) and π^-- (c) induced interactions obtained with the default and new evaporation models are compared to experimental data [10]. In addition the response (cross section multiplied by the energy spectrum as shown in Fig. 2a) is given (arbitrary units). (d) The FLUKA cross sections for proton-, neutron- and pion-induced reactions calculated with the new evaporation model are shown.

interactions above 10 GeV contribute to the measured specific activities, as expected from the significant fluence of high energy particles at the downstream irradiation location of the copper sample (see Fig. 2). Furthermore, Fig 5d) shows that below energies of a few 100 MeV the ^{54}Mn cross section of pion-induced interactions is significantly larger than that one of proton- and neutron-induced interactions, in agreement with the result of the parent reaction scoring given in Table V.

Gamma-emitting isotopes with long half-lives are particularly important for radioactive waste studies. In the present benchmark experiment only a few have been identified due to the relatively short irradiation period of one week. For one of them (^{60}Co from copper) cross sections have been calculated and are shown together with experimental data in Fig. 6. The comparison suggests that FLUKA underestimates the measured cross section at low energy whereas it is

overestimated in the GeV-range. Over- and underestimates seems to cancel each other such that the total production is well predicted, as indicated by this study (ratio of calculated and measured specific activity of 0.84, see Table II). The response curve for proton-induced reactions (see Fig. 6a) covers a rather wide energy range from about 50 MeV up to several tens of GeV. Figure 6b) shows the calculated cross sections for proton-, neutron and pion-induced interactions. The neutron cross section is truncated at the upper energy threshold for low-energy neutron interactions of 19.6 MeV. Below that value experimental data are used, which are not shown here (see discussion in Sec. 3.1).

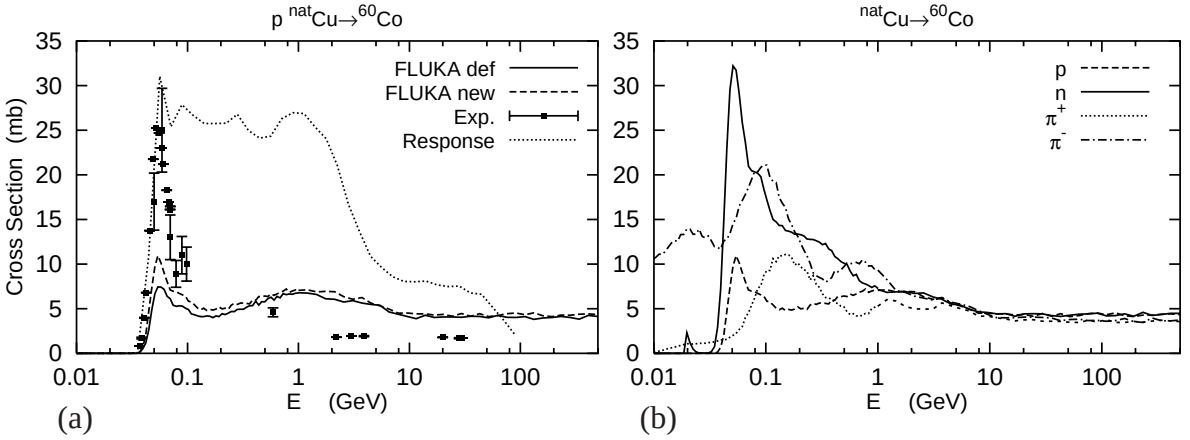

Figure 6: Cross sections for the production of ^{60}Co from natural copper. (a) FLUKA-predictions for proton-induced interactions obtained with the default and new evaporation models are compared to experimental data [10]. In addition the response (cross section multiplied with the energy spectrum as shown in Fig. 2a) is given (arbitrary units). (b) The FLUKA cross sections for proton-, neutron- and pion-induced reactions calculated with the new evaporation model is shown.

5.3 Folding of Particle Fluence with Cross Sections

In case that radionuclides are mainly produced on trace elements in a given material the results of a direct calculation of the isotope yield often show significant statistical uncertainties. However, knowing the average particle energy spectra in the sample together with the corresponding cross sections for the production of the isotope allows the calculation of the specific activity by folding of the latter two quantities. Of course, the method requires the knowledge of the target nucleus which, unless it is obvious, has to be determined from the simulation. In addition, the energy spectra have to be computed for all particles types in the cascade which contribute to the total isotope yield.

In the present study isotope production in the samples was assumed to be caused mainly by protons, neutrons and charged pions and, thus, energy spectra only of these particle types were calculated. The direct calculation of isotope production showed that the remaining contribution by other particles (*e.g.*, kaons) was typically below 10% (see Table V). In the following only two examples are given.

The direct calculation of the specific activity of ^{22}Na in the aluminum sample resulted in a value of 0.278 Bq/g (see Table IV). Folding of protons, neutrons and charged pion spectra with the corresponding cross sections results in a activity of 0.216 Bq/g. Taking into account that other particles for which energy spectra were not calculated contribute about 4.8% and that 4.3% of the yield is produced in interaction on trace elements in the aluminum sample (see Table V) the re-scaled activity is 0.261 Bq/g$\times$1.091=0.285 Bq/g, in good agreement with the value obtained with the direct calculation (ratio of 1.03).

As a second example, ^{48}Cr has been identified by gamma spectrometry in the concrete sample (specific activity of 0.011 Bq/g), but was excluded from the list of FLUKA results due to large statistical uncertainties of the direct simulation. The simulation indicated that the isotope is produced on the iron component in the concrete sample, thus, interaction cross sections on natural iron were assumed in the folding method. The latter results in a specific activity from proton, neutron and charged pion interactions of 0.0077 Bq/g or a ratio of 0.7 between calculated and measured activity. Again, other particles and trace element might contribute, accounting at least in part for the remaining activity of 30% as compared to the measured value.

Figure 7 shows the cross section used in the folding procedure and illustrates that the probability for the production of ^{48}Cr in concrete is low not only due to the small mass fraction of iron (0.69%) but also as a result of the small cross section for the production of ^{48}Cr on iron.

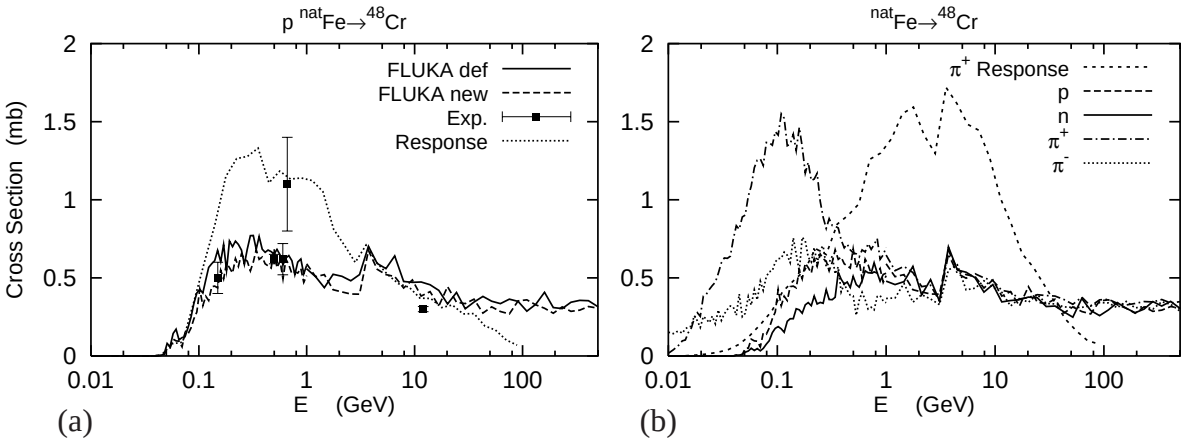

Figure 7: Cross section for the production of ^{48}Cr from natural iron (trace element in the concrete sample). (a) FLUKA-predictions for proton-induced interactions obtained with the default and new evaporation models are compared to experimental data [10]. In addition the response (cross section multiplied with the energy spectrum as shown in Fig. 2a) is given (arbitrary units). (b) The FLUKA cross sections for proton-, neutron- and pion-induced reactions calculated with the new evaporation model is shown together with the response curve for positively charged pions.

5.4 Isomeric States

As discussed in Sec. 3.3 FLUKA cannot predict the production of different isomers of the same isotope. Thus, in the post-processing step the total yield is assumed to be shared equally between the different isomers and the ground state of the isotope and the radioactive build-up and decay are calculated correspondingly. This might cause significant discrepancies between measured and calculated activities in certain cases.

Therefore, the sensitivity of the results to the above assumption has been studied for two examples, ^{44}Sc/^{m44}Sc and ^{52}Mn/^{m52}Mn, respectively. The fraction x of the calculated yield assigned to the isomer and to the ground state of the respective isotope was kept as free parameter and was varied between zero (zero yield for the isomer at production) and unity (zero yield for the ground state at production) in the calculation of the specific activity. The resulting ratios between calculated and measured activities (new evaporation model) are shown in Fig. 8. Here, the value for $x = 0.5$ ("equal sharing") refers to the result quoted in the above tables. As can be seen,

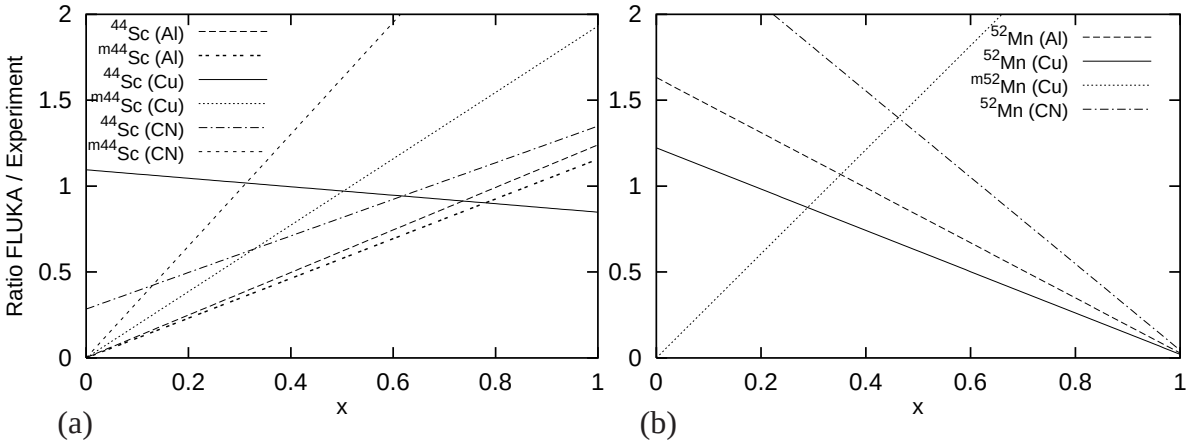

Figure 8: Ratio of calculated and measured specific activities of ^{44}Sc/^{m44}Sc (a) and ^{52}Mn/^{m52}Mn (b) as function of the sharing-fraction x of the calculated total specific activity between the isomer and the ground state of the isotope. Results are given for the three samples subject of this study.

except for the specific activity of ^{44}Sc from copper all results are strongly dependent on the fraction x. If the gamma spectrometry measurement is capable of distinguishing between isomers and ground state the correct fraction could be determined from the data. Unfortunately, the latter is often difficult in cases where half-lives are very different or lines emitted by the isomers overlap with those emitted by the ground state.

Assuming that both the activity of isomer and the ground state are measured with comparable uncertainty the actual fraction x could be determined from the graph as the value at which both lines cross each other. In case of ^{44}Sc/^{m44}Sc (see Fig. 8a) the value would be around 0.15 for the concrete sample (production on iron traces and calcium), implying a general underestimation of the production of ^{44}Sc by FLUKA, and 0.5 for copper. Due to the long cooling time for the measurement of the aluminum sample (1d 16h) ^{44}Sc originates entirely from ^{m44}Sc decays and the value of x cannot be derived. In case of ^{52}Mn/^{m52}Mn both isomer and ground state were only

simultaneously measured in the copper sample for which a value of $x \approx 0.3$ is obtained from Fig. 8b).

6 CONCLUSIONS

An earlier study of benchmarking radionuclide production with FLUKA has been extended by a detailed analysis of reaction channels and radioactive decay chains leading to the measured isotopes. In addition, the energy ranges of the interactions tested with the irradiation experiment were determined by folding of fluence spectra with calculated nuclide production cross sections. This information together with FLUKA results of high statistical significance allows one to draw specific conclusions on the quality of the FLUKA models in the calculation of nuclide production cross sections.

As the study focused on demonstrating the analysis methods, only three materials (aluminum, concrete and copper) of the benchmark experiment were selected. The analysis showed that FLUKA is capable of predicting the production of most of the nuclides identified by the gamma spectrometry analysis to within 30% of the measured activities. It underlines the importance of reducing uncertainties in both measurements and simulations to below this value in order to allow for a meaningful benchmark of FLUKA.

Furthermore, the simulations were repeated using a new implementation of the fragmentation of excited nuclei which includes the evaporation of fragments with mass-numbers up to 24. As expected, the new model improves significantly the predictions for the production of nuclei with masses well below the one of the parent nucleus (*e.g.,* ^{7}Be).

The methods and strategies investigated in the present study will now be applied systematically to all 14 materials of the benchmark experiment contributing to a detailed validation of FLUKA predictions for radionuclide production around high-energy accelerators.

7 ACKNOWLEDGMENTS

The authors are grateful to Alberto Fassò and Alfredo Ferrari for many stimulating discussions.

8 REFERENCES

1. A. Fassò, A. Ferrari and P. R. Sala, "Electron-photon transport in FLUKA: status," *Proceedings of the Monte Carlo 2000 Conference,* Lisbon, Portugal, 23-26 October 2000, A. Kling, F. Barao, M. Nakagawa, L. Tavora, P. Vaz eds., Springer-Verlag Berlin, pp. 159-164 (2001).
2. A. Fassò, A. Ferrari, J. Ranft and P. R. Sala, "FLUKA: Status and Prospective for Hadronic Applications," *Proceedings of the Monte Carlo 2000 Conference,* Lisbon, Portugal, 23-26 October 2000, A. Kling, F. Barao, M. Nakagawa, L. Tavora, P. Vaz eds., Springer-Verlag Berlin, pp. 955-960 (2001).
3. A. Mitaroff and M. Silari, "The CERN-EU high energy reference field facility for dosimetry at commercial flight altitudes and in space," *Radiat. Prot. Dosim.*, **102**, pp. 7-22 (2002).

4. M. Brugger, Y. Donjoux, A. Mitaroff and S. Roesler, “Measurement and simulation of induced activity at the CERN-EU high energy reference field facility,” *Proceedings of the Sixth International Meeting on Nuclear Applications of Accelerator Technology,* San Diego, CA, U.S.A., 1-5 June 2003, pp. 391-398 (2003).
5. M. Brugger *et al.*, “Benchmark studies of induced radioactivity produced in LHC materials, Part I: Specific activities,” *Proceedings of the 10th International Conference on Radiation Shielding, ICRS-10,* Funchal (Madeira), Portugal, 9-14 May 2004, to be published.
6. L. A. Currie, “Limits for qualitative detection and quantitative determination,” *Anal Chem.*, **40**, p. 586 (1968).
7. F. Ballarini *et al.*, “Nuclear models in FLUKA: present capabilities, open problems and future improvements,” *Proceedings of the International Conference on Nuclear Data for Science and Technology, ND2004,* Santa Fe, NM, U.S.A., 26 September-1 October 2004 , to be published.
8. A. Ferrari, Fortran program `preex`, private communication (2003).
9. A. Ferrari, Fortran program `usrsuwevo`, private communication (1999).
10. Landold-Börnstein, *Zahlenwerte und Funktionen aus Naturwissenschaft und Technik, Band 13: Radionuclidproduktion bei mittleren Energien,* Springer-Verlag, Berlin (1991).

Table I: Elemental composition (weight fraction in percent) of the samples as determined by various external companies (EA and EMPA) and by an external institute (EIG) and as used in the simulation (abbreviated by "Simul."). In addition the densities of the different materials are given.

Concrete 1.7 g/cm^3		Copper 8.9 g/cm^3		Aluminum 2.7 g/cm^3				
	EMPA/Simul.		EIG/Simul.		EA	EMPA	EIG	Simul.
O	47.87	Cu	99.328	Al	96.545	96.19	96.69	96.4589
Si	4.0	S	0.0137	Cr	0.039	0.03	0.03	0.033
Ca	35.4	Pb	0.002	Cu	0.123	0.12	0.101	0.115
Al	0.97	Bi	0.001	Fe	0.523	0.59	0.384	0.5
Na	0.03	P	0.0004	Mg	0.85	0.93	0.709	0.83
Fe	0.69	Cd	0.004	Mn	0.725	0.79	0.574	0.696
H	0.6	Zn	0.002	Si	0.994	0.99	1.25	1.08
C	9.24	Se	0.0011	P	–	–	0.0126	0.0126
Mg	0.64	Te	0.002	S	–	–	0.0076	0.0076
K	0.26	Al	0.4745	Cl	–	–	0.0087	0.0087
P	0.03	Si	0.130	Ca	–	–	0.0201	0.0201
S	0.15	Cr	0.0021	Ti	0.03	0.03	0.0305	0.0302
Ti	0.06	Fe	0.0261	Zn	0.09	0.15	0.0732	0.1044
Mn	0.01	Sn	0.002	Ga	–	–	0.0102	0.0102
Sr	0.05	Ni	0.001	Ni	0.013	0.01	0.0154	0.0128
		Mn	0.0016	V	–	$<$0.01	0.0041	0.0041
		Sb	0.004	Zr	–	$<$0.01	0.0024	0.0024
		As	0.002	Cd	–	$<$0.01	–	–
		Ag	0.002	Sn	0.019	$<$0.01	0.0366	0.0278
		Co	0.0002	Pb	0.028	0.12	0.0294	0.0287
				Bi	0.017	$<$0.01	0.0151	0.0161
				Am	–	–	0.0014	0.0014

Table II: Comparison of measured and calculated specific activities in the copper sample for the following cooling times t_c: (1) 34m, (2) 1h 7m, and (3) 48d 3h 21m. In addition to the experimental values, the ratios of the latter and the MDA are given. FLUKA results are listed for both the default and the new evaporation model together with the ratio of calculated and measured activities. All errors are given in percent.

t_c	Isotope	Experiment		MDA	FLUKA def				FLUKA new			
		(Bq/g)	(%)	ratio	(Bq/g)	(%)	ratio	(%)	(Bq/g)	(%)	ratio	(%)
3	^{7}Be	1.29	12.6	12.0	0.058	4.5	0.05	17.1	1.89	0.5	1.47	13.1
3	^{22}Na	0.029	14.3	5.6	0.019	2.5	0.66	16.8	0.02	1.4	0.71	15.7
2	^{24}Na	14.8	8.5	121.0	3.94	2.0	0.27	10.5	7.2	1.0	0.49	9.5
1	^{42}K	21.6	15.3	6.8	12.7	1.7	0.59	17.0	14.1	1.0	0.65	16.3
2	^{43}K	6.38	11.1	11.4	4.19	2.5	0.66	13.6	5.4	1.5	0.85	12.6
2	^{43}Sc	24.6	24.1	9.2	15.9	1.4	0.65	25.5	11.2	1.0	0.45	25.1
2	^{44}Sc	41.1	31.1	88.0	52.7	0.7	1.28	31.8	39.9	0.5	0.97	31.6
2	^{m44}Sc	18.4	13.0	27.8	23.6	0.7	1.28	13.7	17.8	0.5	0.97	13.5
3	^{46}Sc	0.865	8.3	128.0	0.769	0.7	0.89	9.0	0.744	0.4	0.86	8.7
2	^{48}Sc	3.16	12.8	18.2	3.64	2.9	1.15	15.7	4.14	1.6	1.31	14.4
3	^{48}V	1.12	7.8	186.0	1.84	0.6	1.65	8.4	1.37	0.5	1.23	8.3
1	^{49}Cr	15.0	24.9	1.2	20.4	1.2	1.36	26.1	13.5	0.9	0.9	25.8
3	^{51}Cr	3.55	12.7	38.7	4.64	0.5	1.31	13.2	3.97	0.3	1.12	13.0
1	^{52}Mn	18.0	7.9	24.9	14.5	0.8	0.81	8.7	11.8	0.4	0.66	8.3
1	^{m52}Mn	9.6	33.0	7.9	17.8	0.8	1.85	33.8	14.6	0.5	1.52	33.5
3	^{54}Mn	1.13	10.2	97.4	1.33	0.5	1.18	10.7	1.34	0.3	1.19	10.5
1	^{56}Mn	27.7	5.8	20.1	21.7	1.3	0.78	7.1	24.5	0.7	0.89	6.5
3	^{59}Fe	0.558	10.4	42.9	0.39	1.8	0.7	12.2	0.432	1.0	0.77	11.4
2	^{55}Co	7.41	10.2	16.1	6.34	2.3	0.86	12.5	5.25	1.5	0.71	11.7
3	^{56}Co	1.20	7.2	127.0	1.39	0.9	1.16	8.1	1.26	0.5	1.06	7.7
3	^{57}Co	1.75	9.9	92.6	1.6	0.5	0.92	10.4	1.51	0.3	0.86	10.2
3	^{58}Co	6.51	10.2	533.6	5.79	0.3	0.89	10.5	5.87	0.2	0.9	10.4
3	^{60}Co	0.172	8.5	9.1	0.137	0.4	0.8	8.9	0.145	0.3	0.84	8.8
1	^{61}Co	52.7	12.3	4.2	44.0	0.9	0.84	13.2	46.3	0.5	0.88	12.8
2	^{57}Ni	4.78	12.1	15.8	4.14	2.7	0.86	14.8	3.87	1.7	0.81	13.8
2	^{65}Ni	3.46	19.3	3.5	5.38	2.4	1.55	21.7	5.04	1.3	1.46	20.6
1	^{60}Cu	16.4	8.7	12.2	13.9	1.2	0.85	9.9	13.0	0.8	0.8	9.5
1	^{61}Cu	165.	27.2	13.2	173.	0.4	1.05	27.6	156.	0.3	0.95	27.5
2	^{64}Cu	595.	13.2	15.1	336.	0.7	0.56	13.9	331.	0.4	0.56	13.6
2	^{62}Zn	5.66	19.9	4.4	6.86	2.4	1.21	22.3	6.24	1.4	1.10	21.3
3	^{65}Zn	0.117	12.0	8.6	0.075	2.5	0.64	14.5	0.073	1.5	0.62	13.5

Table III: As in Table II, here for the concrete sample and the following cooling times: (1) 11h 41m, (2) 12d 6h 40m, and (3) 55d 2h 31m.

t_c	Isotope	Experiment		MDA	FLUKA def				FLUKA new			
		(Bq/g)	(%)	ratio	(Bq/g)	(%)	ratio	(%)	(Bq/g)	(%)	ratio	(%)
3	^{7}Be	2.95	11.9	263.4	2.63	0.7	0.89	12.6	3.44	0.3	1.17	12.2
3	^{22}Na	0.061	9.9	101.5	0.06	1.1	0.98	11.0	0.053	0.6	0.86	10.5
1	^{24}Na	5.55	3.6	767.6	16.4	53.3	2.96	56.9	3.49	0.7	0.63	4.3
1	^{42}K	1.03	6.1	20.3	1.27	6.9	1.2	13.0	1.25	1.8	1.21	7.9
1	^{43}K	1.52	3.4	157.7	1.6	2.8	1.05	6.2	1.76	1.6	1.16	5.0
1	^{47}Ca	0.343	14.5	29.6	0.237	5.5	0.69	20.0	0.279	3.1	0.81	17.6
1	^{44}Sc	0.321	6.2	12.0	0.301	4.5	0.94	10.7	0.259	2.9	0.81	9.1
1	^{m44}Sc	0.126	11.9	15.5	0.237	4.9	1.88	16.8	0.205	3.2	1.63	15.1
1	^{47}Sc	0.325	8.3	35.0	0.284	5.2	0.87	13.5	0.293	3.1	0.9	11.4
2	^{48}V	0.045	8.8	36.4	0.082	5.9	1.82	14.7	0.069	3.1	1.53	11.9
2	^{51}Cr	0.085	15.8	4.8	0.112	3.9	1.31	19.7	0.114	2.2	1.34	18.0
1	^{52}Mn	0.110	4.1	15.1	0.16	6.4	1.46	10.5	0.156	2.9	1.42	7.0
3	^{54}Mn	0.015	11.9	9.5	0.016	4.1	1.03	16.0	0.016	2.0	1.04	13.9
2	^{56}Co	0.0029	21.8	2.3	0.0023	16.8	0.78	38.6	0.0024	10.0	0.83	31.8

Table IV: As in Table II, here for the aluminum sample and the following cooling times: (1) 1d 16h 55m, (2) 16d 8h 56m, and (3) 51d 9h 47m.

t_c	Isotope	Experiment		MDA	FLUKA def				FLUKA new			
		(Bq/g)	(%)	ratio	(Bq/g)	(%)	ratio	(%)	(Bq/g)	(%)	ratio	(%)
3	^{7}Be	0.789	12.6	20.4	0.287	3.6	0.36	16.2	0.566	1.5	0.72	14.1
3	^{22}Na	0.365	9.6	94.8	0.307	1.2	0.84	10.8	0.278	0.7	0.76	10.3
1	^{24}Na	38.6	3.6	821.3	32.9	0.4	0.85	4.0	31.4	0.3	0.81	3.9
1	^{44}Sc	0.115	23.6	2.1	0.158	12.5	1.37	36.1	0.141	8.8	1.23	32.4
1	^{m44}Sc	0.115	23.6	2.1	0.149	12.6	1.30	36.2	0.133	8.8	1.16	32.4
2	^{46}Sc	0.025	15.7	5.2	0.015	10.1	0.62	25.8	0.015	6.2	0.62	21.9
1	^{47}Sc	0.163	10.6	6.0	0.161	17.1	0.99	27.7	0.181	10.2	1.11	20.8
1	^{48}V	0.199	7.4	5.0	0.185	10.6	0.93	18.0	0.158	6.6	0.8	14.0
2	^{51}Cr	0.257	16.8	4.8	0.233	6.3	0.91	23.1	0.234	3.8	0.91	20.6
1	^{52}Mn	0.224	5.6	8.3	0.238	9.3	1.06	14.9	0.195	5.8	0.87	11.4
3	^{54}Mn	0.081	11.4	17.7	0.078	3.5	0.97	14.9	0.078	2.2	0.97	13.6
3	^{57}Co	0.0042	32.3	1.3	0.0035	17.6	0.83	49.9	0.031	11.7	0.72	44.0
2	^{58}Co	0.019	21.6	3.7	0.015	11.6	0.77	33.2	0.014	3.2	0.71	29.1

Table V: Production channels of selected radionuclides. High energy reaction channels are defined as interactions caused by charged hadrons of any energy and by neutrons with energies above 19.6 MeV. In this case, contributions (in percent) from interactions on a certain target nucleus are given separately for different projectiles (protons, neutrons, pions and other hadrons). In addition, the total contribution of this target nucleus to all high energy reactions is listed. Furthermore, the contribution of low energy neutron interactions to the production of the respective radionuclide is specified. The last column indicates indirect contributions through radioactive decays of other nuclides. Their contribution is given in percent.

Isotope	$t_{1/2}$	High energy reaction (%)							low-E n (%)	decay
			tot	p	n	π^+	π^-	oth.		
^{7}Be	53.29d	^{27}Al	97.6	10.1	11.5	37.2	34.7	4.1	–	–
^{22}Na	2.6y	^{27}Al	95.7	16.1	33.8	18.1	22.9	4.8	–	^{23}Al, ^{22}Mg (<1%)
^{44}Sc	3.93h	^{56}Fe	27.3	0.0	6.8	11.4	4.5	4.5	–	^{m44}Sc ($\approx$ 100%)
		^{55}Mn	52.2	13.6	9.1	13.6	13.6	2.3		^{44}Ti (<1%)
		^{54}Fe	6.9	2.3	2.3	2.3	0.0	0.0		
		^{48}Ti	4.5	4.5	0.0	0.0	0.0	0.0		
^{52}Mn	5.59d	^{56}Fe	34.6	5.9	13.9	4.9	7.9	2.0	–	^{52}Fe, ^{m52}Mn (58%)
		^{55}Mn	48.5	9.9	33.7	2.9	2.0	0.0		
^{7}Be	53.29d	^{63}Cu	56.0	3.5	1.9	27.1	12.7	10.8	–	–
		^{65}Cu	22.2	1.9	0.5	11.1	4.1	4.6		
		^{27}Al	16.0	1.9	1.4	5.7	4.6	2.4		
^{54}Mn	312.12d	^{63}Cu	70.6	6.6	9.3	22.1	23.1	9.5	–	–
		^{65}Cu	29.3	2.5	2.9	10.4	9.3	4.2		
^{60}Co	5.27y	^{63}Cu	50.2	4.8	17.4	9.1	14.5	4.2	9.7	^{m60}Co (50%)
		^{65}Cu	49.8	4.2	11.5	11.6	16.4	6.1		^{60}Mn, ^{60}Fe (<1%)
^{57}Ni	35.60h	^{63}Cu	88.2	19.3	11.6	28.3	18.5	10.5	–	^{57}Cu (<1%)
		^{65}Cu	11.9	1.5	1.1	4.9	3.1	1.3		
^{61}Cu	3.33h	^{63}Cu	88.6	17.9	26.2	21.2	14.5	8.8	–	^{61}Zn (<1%)
		^{65}Cu	11.3	2.7	2.8	2.9	1.6	1.3		
^{64}Cu	12.70h	^{65}Cu	100	18.4	38.8	21.2	19.0	2.6	45.9	–